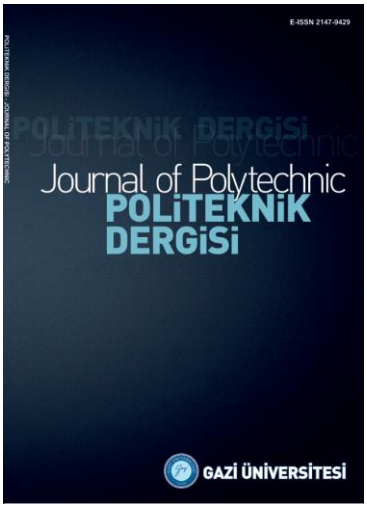

POLİTEKNİK DERGİSİ

JOURNAL of POLYTECHNIC

ISSN: 1302-0900 (PRINT), ISSN: 2147-9429 (ONLINE)
URL: http://dergipark.org.tr/politeknik

Energy efficiency improvements in wind energy systems via sensorless soft-switching control

Rüzgar enerjisi sistemlerinde enerji verimliliğinin sensörsüz yumuşak anahtarlama kontrolü ile geliştirilmesi

***Yazar(lar) (Author(s))**: Tufan Volkan KÜÇÜK[1], Selim ÖNCÜ[2]*

ORCID[1]: 0000-0002-2456-5706

ORCID[2]: 0000-0001-6432-0634

To cite to this article: Küçük T., V. and Öncü S., "Energy Efficiency Improvements in Wind Energy Systems via Sensorless Soft-Switching Control", ***Journal of Polytechnic***, 28(4): 1243-1254, (2025).

Bu makaleye şu şekilde atıfta bulunabilirsiniz: Küçük T., V. ve Öncü S., "Energy Efficiency Improvements in Wind Energy Systems via Sensorless Soft-Switching Control", ***Politeknik Dergisi***, 28(4): 1243-1254, (2025).

Erişim linki (To link to this article): http://dergipark.org.tr/politeknik/archive

DOI: 10.2339/politeknik.1586835

Energy Efficiency Improvements in Wind Energy Systems via Sensorless Soft-Switching Control

Highlights

- *Power control based on regular pulse density modulation for a series DC-DC resonant converter.*
- *Sensorless MPPT of small-scale WECS.*
- *Increasing efficiency by reducing switching losses with soft switching.*

Graphical Abstract

This study examines a small-scale direct-drive wind energy conversion system (WECS) operating under soft switching conditions and utilizing sensorless control.

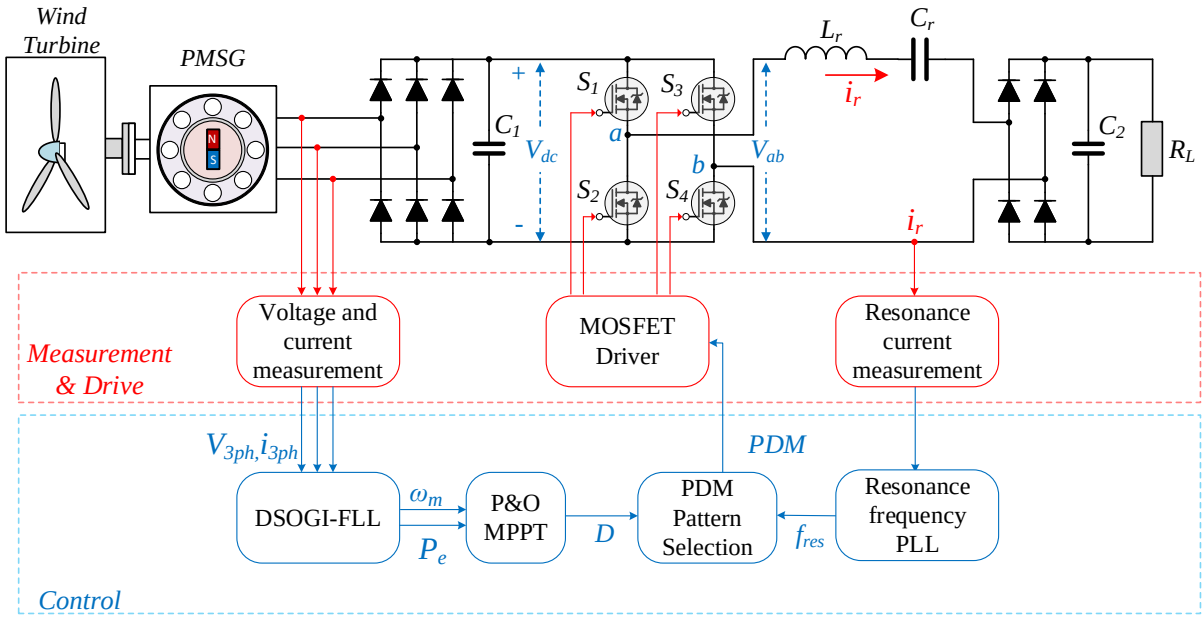

Figure. Proposed wind energy conversion system block diagram

Aim

This work aims to minimize switching losses and enhance system efficiency by implementing a resonant converter in a wind energy conversion system. The article also investigates a sensorless control methodology to reduce costs and increase the system's reliability.

Design & Methodology

The design process is based on an efficient, reliable, low-cost, and high-power density series resonant converter that is compatible with the aerodynamic structure of the wind turbine.

Originality

This study makes an important contribution to literature by examining the coordination of sensorless control, soft switching, and maximum power point tracking in wind energy systems.

Findings

According to the analysis results, it is seen that the overall MPPT efficiency is above 94% and the soft switching state is maintained in the entire load range.

Conclusion

The analysis results demonstrate the efficient and reliable implementation of the wind energy conversion system using a PDM-controlled series resonant converter.

Declaration of Ethical Standards

The authors of this article declare that the materials and methods used in this study do not require ethical committee permission and/or legal-special permission.

Energy Efficiency Improvements in Wind Energy Systems via Sensorless Soft-Switching Control

Research Article / Araştırma Makalesi

Tufan Volkan KÜÇÜK[1,2*], Selim ÖNCÜ[3]

[1] The Institue of Graduate Programs, PhD., Karabuk University, Turkey
[2] Osmaneli Vocational High School, Department of Electric, Bilecik Seyh Edebali University, Turkey
[3] Faculty of Engineering, Department of Electrical and Electronics Eng., Karabuk University, Turkey

(Geliş/Received : 17.11.2024; Kabul/Accepted : 15.12.2024 ; Erken Görünüm/Early View : 30.01.2025)

ABSTRACT

This study implements a series resonant converter (SRC) and pulse density modulation (PDM) power control strategies to minimize switching losses and improve the efficiency of an off-grid, small-scale wind energy conversion system (WECS). Additionally, the maximum power point tracking (MPPT) method was employed to further reduce costs and increase system reliability. The "perturb and observe" (P&O) MPPT technique was utilized, enabling operation at the maximum power point (MPP) without the need for wind speed data or an aerodynamic model of the turbine. The speed and power data required for the P&O algorithm were derived from the three-phase generator variables using the double second-order generalized integrator frequency-locked loop (DSOGI-FLL) algorithm. The performance of a 1.5 kW WECS was analyzed through simulations conducted in Powersim (PSIM), and the results are presented. The analysis revealed that the designed system achieved an average MPPT efficiency of 97%. Furthermore, the efficiency of the resonant converter was measured to be 90% for the lowest wind speed and 93% for other wind speeds. These findings demonstrate that the proposed system offers a significant improvement in overall energy conversion efficiency, ensuring reliable and cost-effective operation of small-scale WECS, with an average system efficiency of approximately 90-93% across varying wind conditions.

Keywords: Wind energy, soft switching, pulse density modulation, sensorless control, DSOGI-FLL.

Rüzgar Enerjisi Sistemlerinde Enerji Verimliliğinin Sensörsüz Yumuşak Anahtarlama Kontrolü ile Geliştirilmesi

ÖZ

Bu çalışmada, anahtarlama kayıplarını en aza indirmek ve şebekeden bağımsız, küçük ölçekli bir rüzgar enerjisi dönüşüm sisteminin (REDS) verimliliğini artırmak için bir seri rezonans dönüştürücü (SRD) ve darbe yoğunluğu modülasyonu (DYM) güç kontrol stratejileri uygulanmaktadır. Ayrıca, maliyetleri daha da düşürmek ve sistem güvenilirliğini artırmak için maksimum güç noktası izleme (MGNİ) yöntemi kullanılmıştır. Rüzgar hızı verilerine veya türbinin aerodinamik modeline ihtiyaç duymadan maksimum güç noktasında (MGN) çalışmayı sağlayan "değiştir ve gözle" (D&G) MGNİ tekniği kullanılmıştır. D&G algoritması için gerekli hız ve güç verileri, çift ikinci dereceden genelleştirilmiş integratör tabanlı frekans kilitlemeli döngü (DSOGI-FLL) algoritması kullanılarak üç fazlı generatör değişkenlerinden türetilmiştir. Powersim'de (PSIM) gerçekleştirilen simülasyonlar aracılığıyla 1,5 kW'lık bir REDS'in performansı analiz edilmiş ve sonuçlar sunulmuştur. Analiz, tasarlanan sistemin ortalama %97 MGNİ verimliliği elde ettiğini ortaya koymuştur. Ayrıca, rezonans dönüştürücünün verimliliği en düşük rüzgar hızı için %90 ve diğer rüzgar hızları için %93 olarak ölçülmüştür. Bu bulgular, önerilen sistemin genel enerji dönüşüm verimliliğinde önemli bir gelişme sağladığını ve değişen rüzgar koşullarında yaklaşık %90-93 ortalama sistem verimliliği ile küçük ölçekli WECS'lerin güvenilir ve uygun maliyetli çalışmasını sağladığını göstermektedir.

Anahtar kelimeler: Rüzgar enerjisi, yumuşak anahtarlama, darbe yoğunluk modülasyonu, sensörsüz control, DSOGI-FLL.

1. INTRODUCTION

The integration of wind energy with technical improvements establishes it as a significant competitor among renewable energy sources. Technological developments have led to enhanced efficiency, reliability, and economic viability of WECS. Small wind turbines are specifically engineered for individual use in distant or off-grid locations, and they play a vital part in achieving energy self-sufficiency. These systems, specifically designed for residential, agricultural, and small-scale uses, enhance local energy production while reducing environmental impact and energy expenses [1-5].

For rectifying the generator voltage in small-scale WECS, simple and low-cost solutions such as diode rectifiers are preferred. In designs employing uncontrolled rectifiers, boost converter configurations are commonly utilized to increase generator voltage for

*Sorumlu Yazar (Corresponding Author)
e-posta : tufan.kucuk@bilecik.edu.tr

supplying the DC bus, owing to their straightforward management and cost-effectiveness [6-9]. In cases where WECS directly feeds a battery with a low voltage level, buck converters can be used [10-12]. However, this design structure can only lower the input voltage, so it cannot meet load requirements under all wind conditions. Therefore, especially in battery-supported applications, buck-boost converters [13-15] and SEPIC converters [16] are more preferred. All of the converters discussed operate under hard switching conditions, which involve instantaneous transitions between on and off states. This results in increased switching losses, primarily owing to the substantial overlap of voltage and current during these transitions, leading to reduced efficieny and increased thermal stress on the components. Furthermore, power switches in these converters are subjected to substantial current and voltage stresses, which not only increase the thermal load but also degrade the reliability and lifespan of the system components over time. Resonant converters operating under soft switching conditions present a more efficient and reliable alternative to hard-switching PWM converters. By reducing switching losses and minimizing switching stress on power switches, soft switching improves overall system efficiency and enhances the reliability of the components, making resonant converters a favorable choice for high-performance applications. In [17], researchers implemented an LCC resonant converter for high-voltage DC transmission in WECS, achieving power control through variable frequency control. In a similar study [18], researchers employed the variable frequency method to analyze power control in high voltage direct current (HVDC) systems, utilizing LLC resonant converters and three-phase boost rectifiers. In [19], a resonant switched capacitor converter used in HVDC transmission systems under zero-current switching (ZCS) condition is analyzed. Power control with variable frequency makes passive circuit elements difficult to design and does not yield successful results under all load conditions. Especially under low-load conditions, resonant converters may transition to hard switching conditions beyond soft switching conditions. A study presented in [20] proposes the combined use of phase shift and variable frequency control methods in a SRC to mitigate the effects of this negative situation. All the aforementioned studies have focused on the realization of power transfer with resonant converters at constant input voltage, and wind turbine dynamics and operation of the system at the MPP are excluded. In [21], a WECS using an LCC resonant converter was proposed, and in [22], a WECS using an LLC resonant converter was proposed. Both designs used frequency modulation for power control, operating the system at MPP for two different wind speeds, but did not analyze performance under low load conditions.

Resonant converters utilize various methods for power control, including frequency modulation, phase shift modulation, PDM, and hybrid combinations of these techniques. In frequency modulation, power regulation is attained through the modulation of the switching frequency, which in turn causes variations in the gain of the SRC. The changing switching frequency complicates the design of magnetic and driver circuits, and depending on the SRC design, soft switching conditions may not be achievable under all load conditions. [23].

Phase shift modulation ensures that power is controlled at a constant switching frequency. This approach, adjusting the relative phase angle of the two switching legs, regulates the input voltage of the SRC, which in turn controls the output voltage. The design of driver and magnetic circuits is made easier when operating at a fixed frequency. However, under light load conditions, the system may lose soft switching capabilities [24]. Unlike the other methods mentioned, pulse density modulation is a way to control power that can work at or near the resonant frequency across the whole load range. This makes soft switching possible under all designed load conditions. This method, when implemented with a fixed switching frequency, selectively eliminates certain switching pulses to achieve power control [23-25].

In this study, a small power WECS using permanent magnet synchronous generator (PMSG) is designed in PSIM with a series resonant DC-DC converter (SRDC). Moreover, its operation at the MPP is achieved through sensorless control. The SRC's power regulation is carried out using the PDM method, which enhances the system's efficiency and reliability.

The goals and objectives of the study are presented below.

- This study is to enhance the efficiency of an off-grid, small-scale WECS by minimizing switching losses. The proposed system, comprising a PMSG, SRDC, and a three-phase diode rectifier, is designed to maintain soft switching conditions across the whole spectrum of wind speeds. In this framework, the SRDC is regulated using the PDM power control method, ensuring the system operates in soft switching mode at the MPP.
- The designed WECS aims to increase the reliability of the designed WECS by reducing the electrical stresses on the SRDC. The PDM method facilitates zero voltage switching (ZVS) and, by operating at the resonant frequency across all conditions, also achieves zero current switching (ZCS).
- The study is to enhance power density while minimizing the cost of the designed system. An increase in switching frequency enables a reduction in the size of passive components.
- The proposed MPPT algorithm is implemented without the use of wind speed, turbine parameters, and mechanical speed/position information. This approach aims to reduce costs and enhance the overall system performance and reliability.

2. PROPOSED WECS

The circuit configuration for the proposed small-scale WECS is presented in Figure 1. The generator employs a three-phase diode rectifier. Tracking the maximum power and energy transfer to the load is realized by SRC. The P&O MPPT algorithm is chosen to ensure continuous operation of the system at the MPP under specified wind speed conditions. Speed and power information, utilized as input data for the P&O algorithm, are obtained using the DSOGI-FLL method. By combining these two algorithms, MPPT can independently be performed on the turbine's aerodynamic model. Power control of the SRC is implemented using the PDM technique. The output variable of the P&O algorithm determines the pulse density [26]. Consequently, power control is achieved under soft-switching conditions, thereby minimizing switching losses.

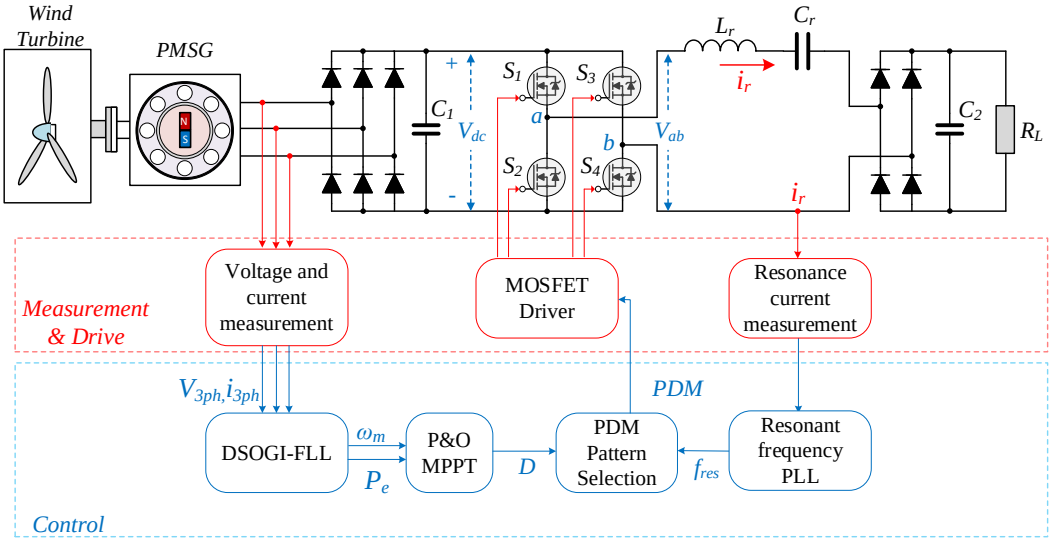

Figure 1. Proposed WECS Block diagram.

2.1. Wind Turbine and PMSG Model

Equation (1) is used to calculate the mechanical power that the wind turbine obtains from the wind. Equation (2) defines the tip speed ratio of the turbine (λ) and Equation (3) expresses the variation of the wind turbine power coefficient [27].

$$P_T = \frac{1}{2}\rho A_r v_w^3 C_p(\lambda) \quad (1)$$

$$\lambda = \frac{\omega_m R_T}{v_w} \quad (2)$$

$$C_p(\lambda,\beta) = 0.5176\left(\frac{116}{\lambda_i} - 0.4\beta - 5\right)e^{-\frac{21}{\lambda_i}} + 0.0068\lambda$$
$$\frac{1}{\lambda_i} = \frac{1}{\lambda + 0.08\beta} - \frac{0.035}{\beta^3 + 1} \quad (3)$$

The variables in the equations are as follows: "R_T" represents the radius of the wind turbine rotor plane (m), "ρ" indicates the air density (kg/m^3), "ω_m" is the turbine shaft speed (rad/s), "A_r" is the area swept by the turbine blades (m^2), "v_w" is the wind speed (m/s), and "C_p" is the turbine power coefficient. The specifications of the turbine and PMSG are detailed in Table 1.

Table 1. Wind turbine and PMSG parameters

Parameter	*Symbol*	*Value*	*Unit*
d-axis inductance	L_d	20.5	mH
Radius of the rotor plane	R_T	1.25	m
q-axis inductance	L_q	20.5	mH
Optimal tip speed ratio	λ_{opt}	8.1	rad
Generator rated power	P_g	2.5	kW
Number of poles	P	10	-
Stator resistance	R_s	1.72	Ω
Maximum power coefficient	C_{p_max}	0.48	-
Air density	ρ	1.2	kg/m^3

2.2. SRDC Converter

The SRDC consists of a resonant inductor (L_r), a full wave rectifier, filter capacitors ($C_1 - C_2$), full-bridge inverter ($S_1 - S_4$) and resonant capacitor C_r. The full-bridge inverter converts the applied direct voltage into a square wave. A resonant circuit enables the conversion of the inverter's output current into a sinusoidal form. The sinusoidal form of the resonant current inherently possesses zero-crossing moments. When the switching operation is executed at the zero-crossing points of the resonant current, zero-current switching (ZCS) may occur, which minimizing switching losses. The SRDC and the equivalent inverter scheme are depicted in Figure

2. The resonant frequency (f_r) is determined in accordance with Equation (4) [30].

$$f_r = \frac{1}{2\pi\sqrt{L_r C_r}} \tag{4}$$

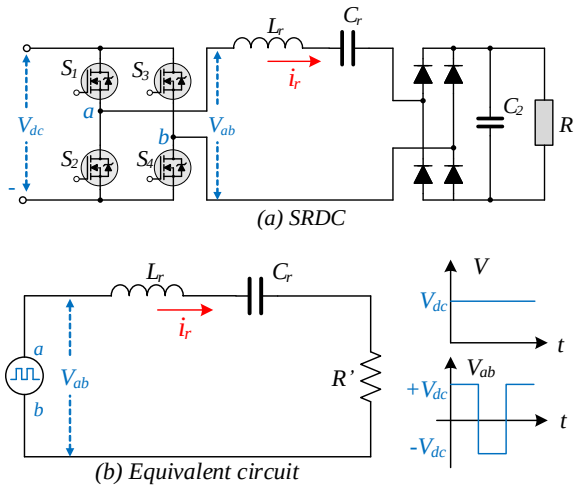

Figure 2. SRDC and equivalent circuit

When the switching frequency (f_{sw}) equals the f_r, the circuit's impedance is minimized. To facilitate the analysis of the SRC, the circuit structure provided in Figure 2 (b) is used. AC equivalent resistance (R') is defined by Equation (5).

$$R' = \frac{8R}{\pi^2} \tag{5}$$

The quality factor (Q) and the time constant (τ) of the SRC are respectively presented in Equations (6) and (7).

$$Q = \frac{(2\pi f_r)L_r}{R'} = \frac{(\omega_r)L_r}{R'} \tag{6}$$

$$\tau = \frac{2Q}{\omega_r} = \frac{2L_r}{R'} \tag{7}$$

2.3. PDM Based Power Control

The PDM is based on controlling the output power by periodically omitting some pulses within a certain pulse group [31]. In the PDM method, the behavior of the resonant current along with the conduction and cut-off states of the power switches are presented in Figure 3. In Mode-1, power switches S_1 and S_4 are conducting, while S_2 and S_3 are in the off state. The voltage V_{ab} is equal to the positive value of the input voltage, $+V_{dc}$. In Mode-II, S_2 and S_3 are on, while S_1 and S_4 are off. The output voltage equals $-V_{dc}$. Mode-III corresponds to the pulse delete duration of PDM. During this mode, S_2 and S_4 switches are conducting, S_1 and S_3 are in the off state. Therefore, V_{ab} is zero, and the resonant current (i_r) exhibits damped oscillatory behavior. The envelope surrounding the i_r in the figure represents its oscillatory amplitude and is denoted by i_E. The maintenance of damped oscillation without the resonant current falling to zero depends on a sufficiently high quality factor ($Q \geq 5$).

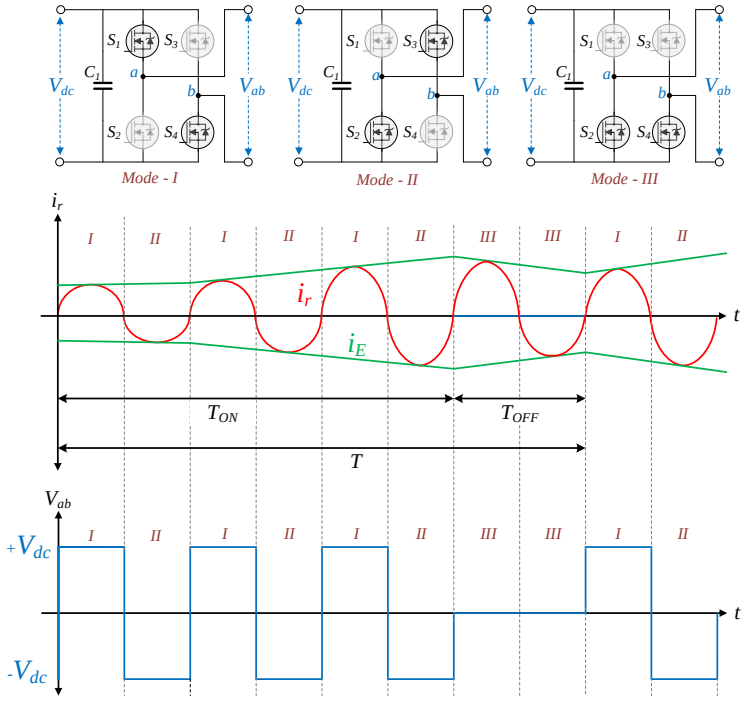

Figure 3. The operating modes of a PDM-controlled resonant converter.

In PDM control, the T_{ON}/T ratio expresses the pulse density (D), where (T_{ON}) is the total duration of modes I and II, and T is the PDM period [31,32]. Figure 4 provides the switching signals and D values for a regular 32-pulse PDM.

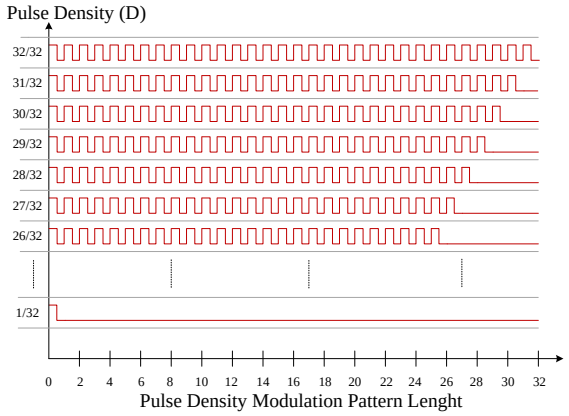

Figure 4. 32 pulse length regular PDM

The determination of the output power for the PDM-controlled SRC, as shown in Equation (8), depends on the D and the τ of the SRC. [31,32].

$$P = \frac{2}{\pi} V_{dc} \cos(\theta) \frac{1}{T} \int_0^{T_{ON}} i_E(t)dt$$

$$P_{max} = \frac{2}{\pi} V_{dc} I_{max} \cos(\theta) \tag{8}$$

$$P = P_{max} \left[\frac{T_{ON}}{T} + \frac{\tau}{T} \left(\frac{1 - e^{-\frac{T_{ON}}{\tau}}}{1 - e^{-\frac{T}{\tau}}} \right) \left(e^{-\frac{T_{ON}}{\tau}} - e^{-\frac{T}{\tau}} \right) \right]$$

P_{max} as expressed in Equation (8) depends on the V_{dc}, the maximum amplitude of the resonant current (I_{max}) when $D = 1$ ($T_{ON} = T$) and the phase angle θ between the output voltage and current of the inverter. When the PDM period is selected to be significantly less than τ of the SRC ($T \ll \tau$), P is directly correlated to the square of the D, as defined by Equation (9).

$$\lim_{\tau \to \infty} P = P_{max} D^2 \tag{9}$$

When the PDM period is significantly larger than the τ of the SRC ($T \gg \tau$), P exhibits a linear relationship with the D. [32].

$$\lim_{\tau \to \infty} P = P_{max} D \tag{10}$$

In the study, a 32-pattern regular PDM method was utilized for power control of the resonant converter. The use of a 32-pattern length specifically enables more precise MPPT compared to 16-pattern and 8-pattern lengths. However, increasing the pattern length leads to a reduction in the PDM frequency and an increase in the amplitude of low-frequency harmonics. This phenomenon may negatively impact EMI (electromagnetic interference) and RFI (radio frequency interference). To mitigate the disadvantages, alternative solutions include increasing the switching frequency when the pattern length is extended or adopting an irregular PDM method instead of the regular PDM method.

2.4. PLL Control for Resonant Frequency

Ideal conditions are employed to ascertain the values of the L_r and C_r. However, during the application, the actual resonant frequency of the circuit may be different from the calculated resonant frequency. PLL method is used to ensure that the switching frequency matches the resonant frequency. The primary function of the PLL circuit is to ascertain the θ angle between i_r and V_{ab} and to adjust the switching frequency to achieve a value of zero [32]. When the switching frequency aligns with the resonant frequency, ZCS condition occurs. Figure 5 shows the PLL block diagram.

3. SENSORLESS CONTROL OF MPPT

Wind and turbine speed information is generally required for the operation of wind turbines at MPP. These mechanical sensors, which must be well calibrated and precise, negatively affect the system cost and reliability. Among the MPPT methods, the P&O algorithm can operate the turbine at MPP without depending on the wind speed information and the parameters of the turbine aerodynamic model. In the P&O method, which is performed without the use of mechanical sensors, the variation of the turbine mechanical speed and power is determined by utilizing the generator output voltage, current and power information.

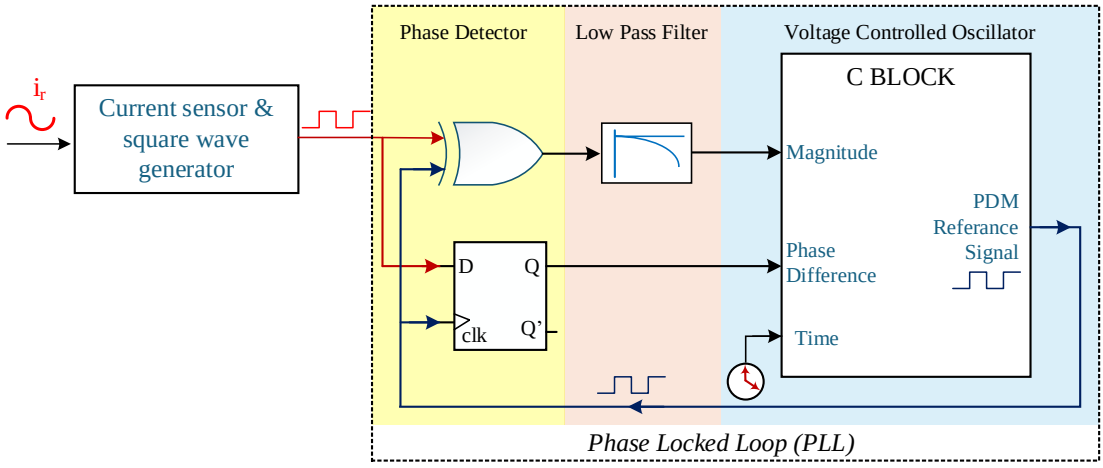

Figure 5. Resonant frequency PLL algorithm

To maintain operation at the MPP, the control variable of the power converter is adjusted in a specified step interval, ensuring the system operates at MPP. In case a diode rectifier is used at the generator output, the generator current and accordingly the output voltage contain high order harmonics. This negatively affects the performance of the P&O algorithm. Due to its easy implementation and good filtering ability, DSOGI-FLL is frequently used for grid synchronization in grids with harmonic distortion [33, 34]. DSOGI-FLL enables the determination of the fundamental components of generator output voltages and currents. Additionally, the FLL structure allows for the determination of the electrical frequency and, consequently, the mechanical speed of the generator. The mechanical speed and power information obtained from DSOGI-FLL constitute the P&O algorithm's input variables. The P&O changes the D value of the SRC to operate the WECS system at MPP.

3.1. DSOGI-FLL

Figure 6 shows the DSOGI-FLL structure. The v_α and v_β components are obtained by Clarke transformation of three phase voltage magnitudes (V_{abc}). These two voltage magnitudes constitute the input values of the SOGI quadrature signal generator. The instantaneous angular frequency calculated by FLL is expressed by "ω'". "v'_α" and "qv'_α" and "v'_β" and "qv'_β" are quadrature output signals. The frequency error signals are denoted by "$e_{v,\alpha}$" and "$e_{v,\beta}$". The adjustable gain value that affects the time response and filtering ability of the SOGI is denoted by "k" [34]. The closed loop transfer functions of SOGI are provided in Equation (11) and (12). $D_{(SOGI)}(s)$ is a band-pass filter and $Q_{(SOGI)}(s)$ is a low-pass filter [35].

$$D_{(SOGI)\alpha,\beta}(s)=\frac{v'_{\alpha,\beta}}{v_{\alpha,\beta}}(s)=\frac{k\omega' s}{s^2+k\omega' s+\omega'^2} \tag{11}$$

$$Q_{(SOGI)\alpha,\beta}(s)=\frac{qv'_{\alpha,\beta}}{v_{\alpha,\beta}}(s)=\frac{k\omega'^2}{s^2+k\omega' s+\omega'^2} \tag{12}$$

In the FLL block presented in Figure 6, the value Γ represents the gain of the FLL. When the fundamental frequency of the input signal is ω, the transfer function and settling time $t_{s(FLL)}$ of the FLL are given by Equation (13) [35].

$$\frac{\omega'}{\omega}=\frac{\Gamma}{s+\Gamma}\rightarrow t_{s(FLL)}\approx\frac{5}{\Gamma} \tag{13}$$

The relationship between the value of ω′ and ω determines the sign of the frequency error values $e_{v,\alpha}$ and "$e_{v,\beta}$. The integral controller gain −Γ regulates ω′ to be equal to ω. In order to regulate the initial conditions of the frequency synchronization, the constant value ω_0 is added to the algorithm. FLL gain is normalized by Equation (14) [36].

$$\frac{k\omega'}{2\left[\left(v_\alpha^+\right)^2+\left(v_\beta^+\right)^2\right]} \tag{14}$$

With the DSOGI-FLL structure, the electrical frequency ω′ of the generator output voltage is estimated. To determine the estimated mechanical speed ω'_m, ω′ is divided by the total number of pole pairs p and calculated as in Equation (15).

$$\omega'_m=\frac{\omega'}{p} \tag{15}$$

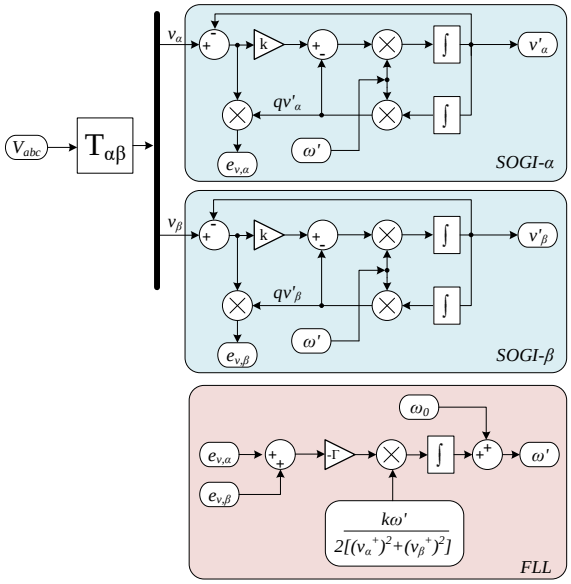

Figure 6. DSOGI-FLL block diagram

(16)

To calculate the fundamental component of the generator active power, DSOGI is applied to the three phase current and voltage quantities separately. Positive sequential components are determined by using the obtained α and β components. The instantaneous active power of the fundamental component is calculated by applying the p-q theory to the obtained positive components [37,38]. The block diagram of the positive-negative sequence calculation and power estimation algorithms is given in Figure 7.

3.2. P&O MPPT

In the proposed P&O method, the estimated generator mechanical speed ω'_m and the estimated fundamental component of generator active power (P_{SOGI}) are utilized as input data for the algorithm. The output data of the algorithm is represented by the D value of the resonant converter. The transferred power by the resonant converter to the load is proportional to the square of D, as expressed in Equation (13). For each specific wind speed value, the wind turbine has a corresponding MPP.

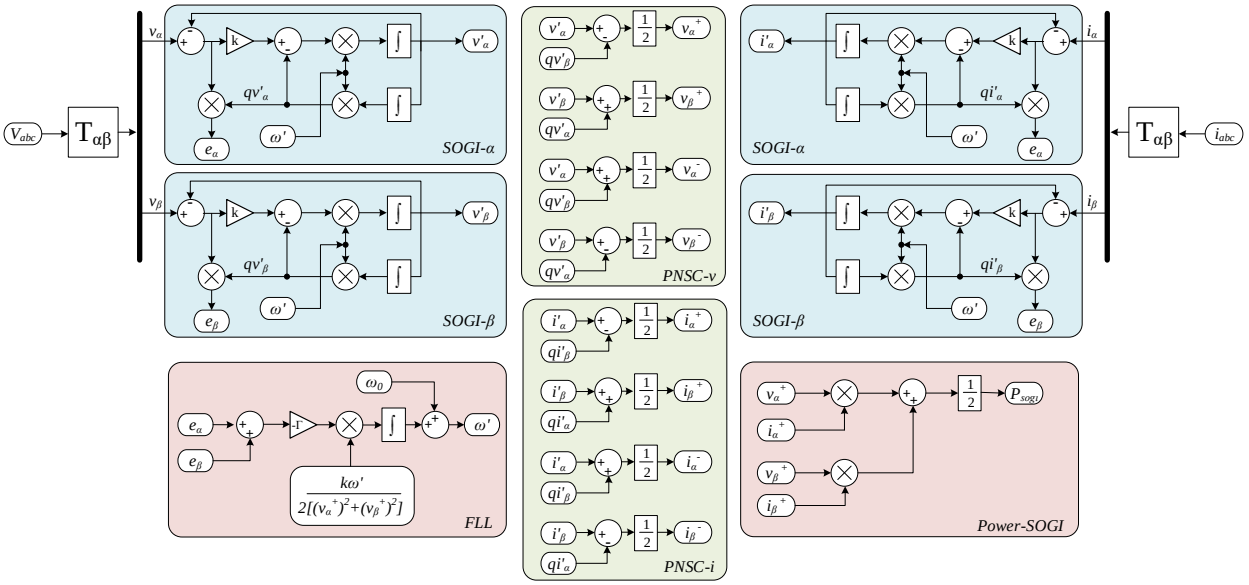

Figure 7. DSOGI-FLL and power calculation block diagrams

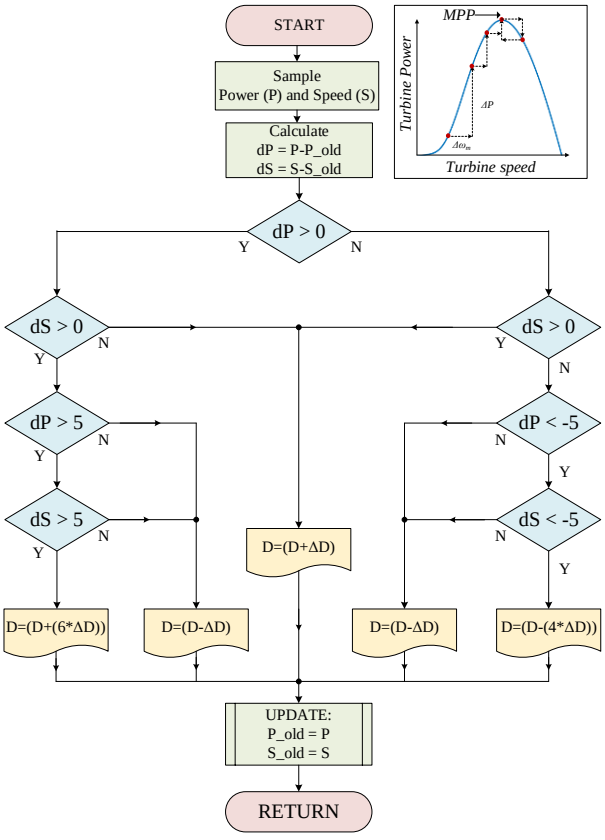

Figure 8. Variable step size P&O

The P&O algorithm adjusts the D value by increasing or decreasing it according to changes in power and speed, thus maintaining the system's operation at the MPP. The change in the D value, denoted as ΔD, represents the step size of the algorithm [39-41]. To boost the efficiency and performance of the system when there are sudden variations in wind speed, the ΔD value is utilized in a variable step way. Proposed P&O algorithm is shown in Figure 8.

4. SIMULATION RESULTS

This article analyzes a sensorless control system designed for a wind turbine employing a direct-drive 1.5 kW PMSG. The simulation assessments were conducted using Powersim software. The novelty of the study lies in the ability of the power converter to operate under soft switching conditions across all load conditions, thereby minimizing switching losses. The P&O for MPPT has been chosen due to its ability to operate independently of turbine parameters. The proposed power converter and control algorithm play a critical role in enhancing the energy efficiency, operational performance, reliability, and power density of the WECS. The results demonstrate that the proposed control strategy responds quickly and accurately to changes in wind speed, maximizing energy production, efficiency and system reliability. Table 2 presents the parameters of the SRC, DSOGI-FLL, PDM and PSIM. The simulation model prepared in PSIM is presented in Figure 9. Figure 10 demonstrates the system's ability to track the MPP under varying wind speed conditions. The MPPT algorithm activates at 0.2 seconds into the simulation, while the generator operates without load prior to this.

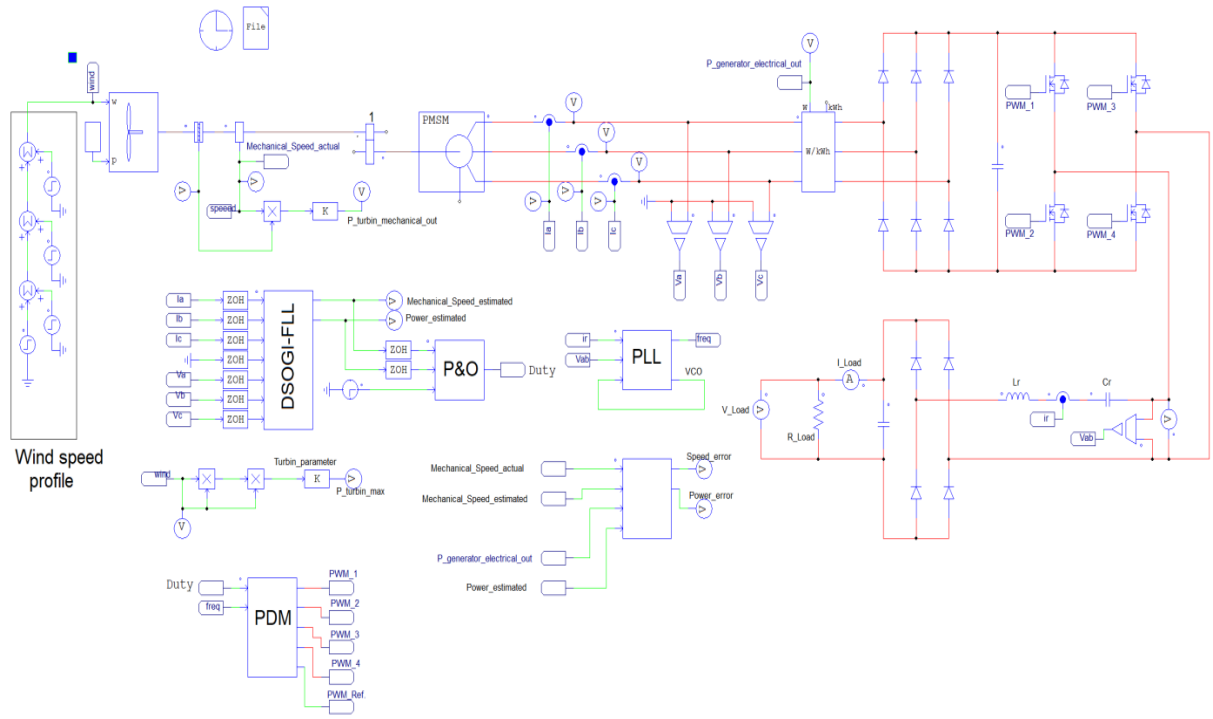

Figure 9. PSIM simulation model

Table 2. Parameters of SRC, PDM algorithm, DSOGI_FLL algorithm and PSIM software

Parameter	*Symbol*	*Value*	*Unit*
Resonant inductor	L_r	1.5	mH
Resonant capacitor	C_r	10.5	nF
Load	R	70	Ω
Resonant frequency	f_{res}	40	kHz
Quality factor	Q	6.64	-
PDM Pattern	-	Regular	-
PDM lenght	-	32	-
Sampling frequency	f_{samp}	20	kHz
DSOGI-FLL k constant	k	1.4142	-
DSOGI-FLL Γ constant	Γ	230	-
DSOGI-FLL ω_o constant	ω_o	100	Rad/s

The estimated mechanical angular speed of the generator (ω'_m) and the electrical output power data obtained from the DSOGI-FLL algorithm are fed into the P&O. The P&O modifies the D value of the SRC by monitoring variations in power and speed to ensure the system functions at the MPP. The turbine's mechanical output power (P_turbin mechanical out) is calculated from the product of the instantaneous speed (ω_m) and torque (T_m) measured from the turbine shaft (P_turbin_mechanical_out = $\omega_m \cdot T_m$). The maximum power output for specified wind speeds of the wind turbine is referred to as P_turbin_max. Figure 11 (a) denotes the power value estimated from the DSOGI-FLL algorithm as Estimated_Power ($P_{\_SOGI}$). The generator's average output power is measured using a three-phase wattmeter in the simulation and is shown on the graph as P_generator_electrical_out. The power error (Power_error) represents the difference between the actual generator output power and the estimated power. Similarly, the speed value estimated from the FLL algorithm, ω'_m, is shown on the graph as Estimated mechanical speed, and the angular speed measured from the generator rotor shaft is denoted as Actual Mechanical speed. Figure 11 (b) presents detailed steady-state views of power and speed error values. For wind speeds of 8 m/s, the power error measured is 18.5 W; for 10 m/s, it is 33 W; for 6 m/s, it is 11 W; and for 9 m/s, it is 25 W. The power error as a percentage of the generator output power is measured as 2.6%, 2.5%, 3.6%, and 2.5%, respectively. The speed error values for the same wind speed profile are measured as 1.03 rad/s, 1 rad/s, 1.02 rad/s, and 1.03 rad/s, respectively. The speed error as a percentage of the actual mechanical speed is calculated as 1.8%, 1.3%, 2.3%, and 1.6%, respectively.

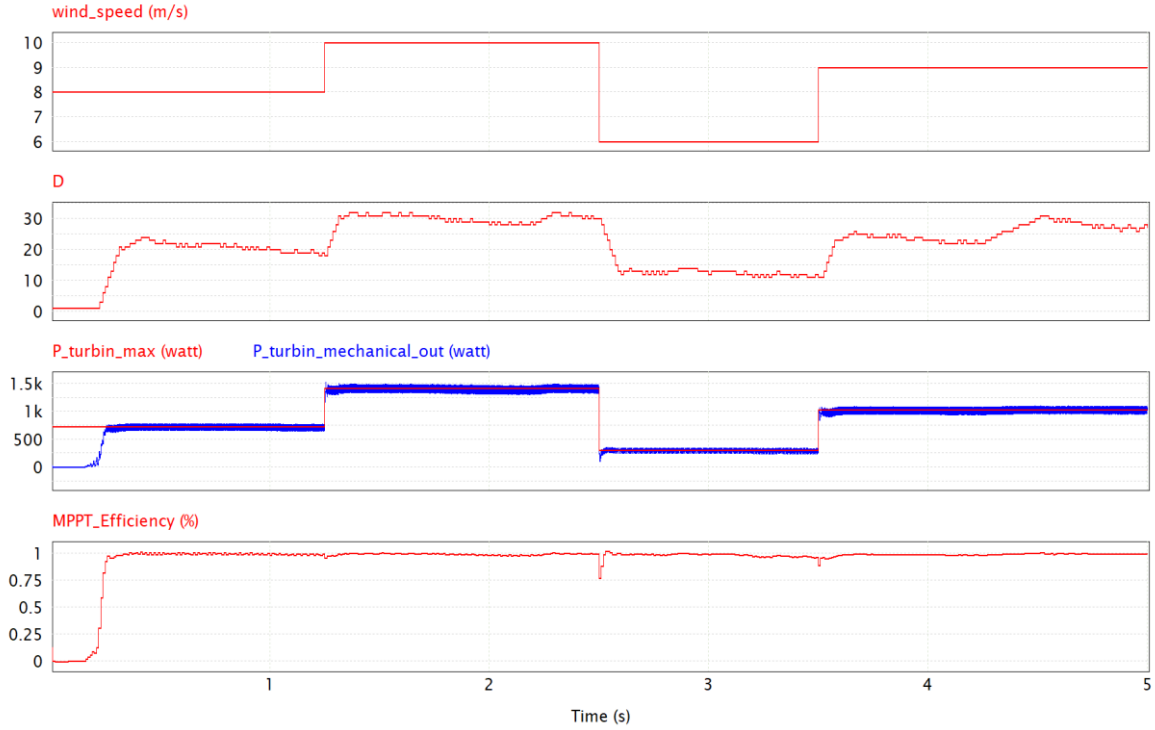

Figure 10. Variation of the MPPT efficiency, turbine mechanical output power, and the theoretical maximum power curves for the turbine, along with changes in the *D* value according to variable wind speeds

The measurements indicate that the error rates are within acceptable levels and demonstrate the success of the DSOGI-FLL algorithm in detecting power and speed values. Figure 12 illustrates the converter voltage and current, operating under soft switching conditions across various wind speeds.

In the figure, the converter's output voltage is denoted as V_{ab}, as illustrated in the circuit structure shown in Figure 2. It is observed that the resonant current maintains a sinusoidal form at all wind speeds, and the resonant current reaches zero during the moments of increase or decrease in V_{ab} voltage.

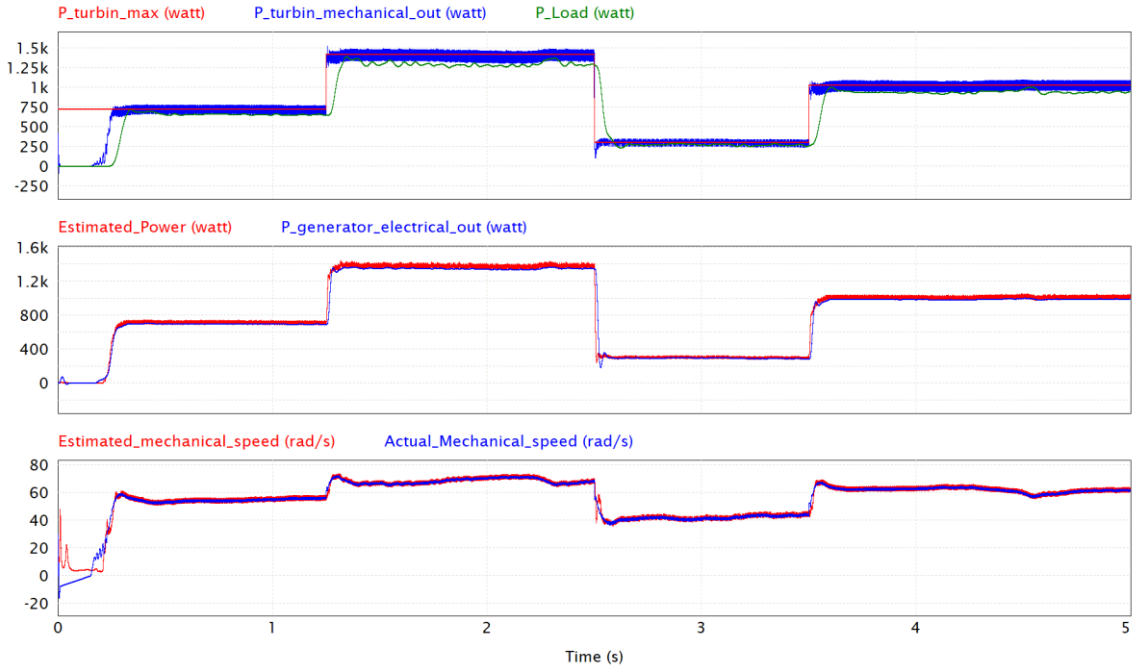

(a)

Figure 11. Plots comparing the real power and speed values with the estimated values

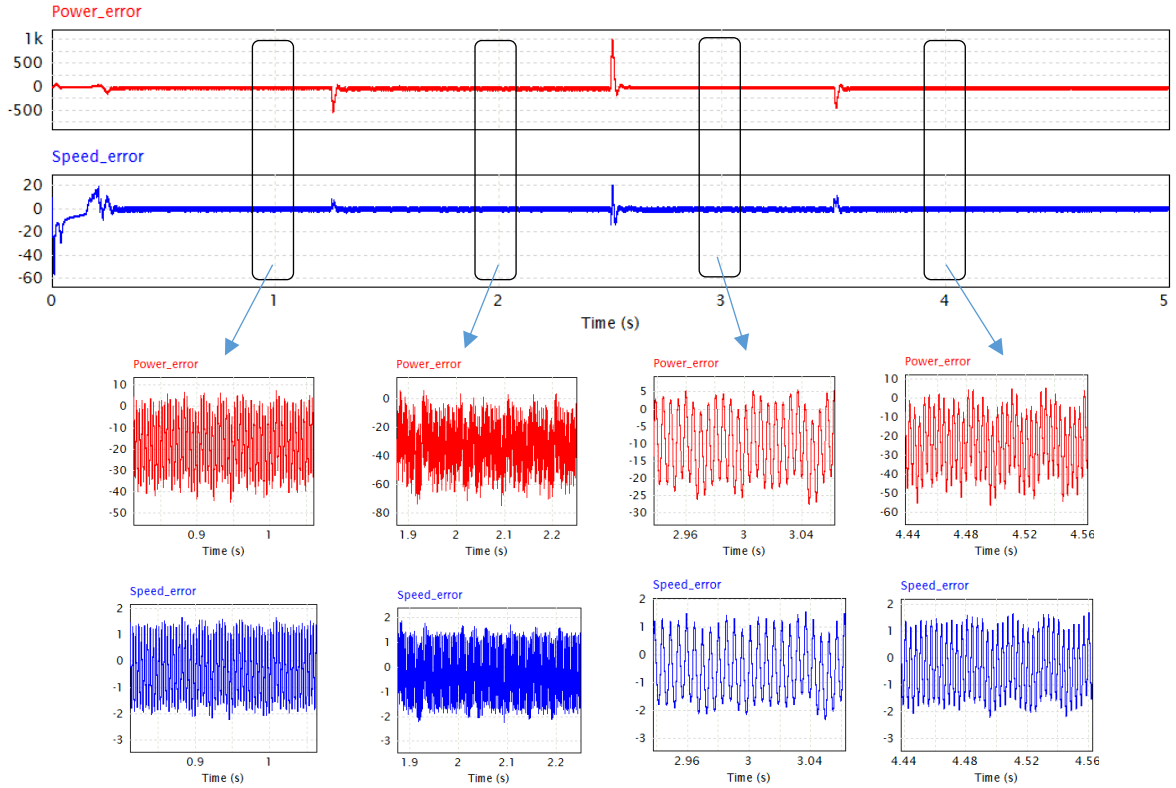

(b)

Figure 11. (Cont.) Plots comparing the real power and speed values with the estimated values

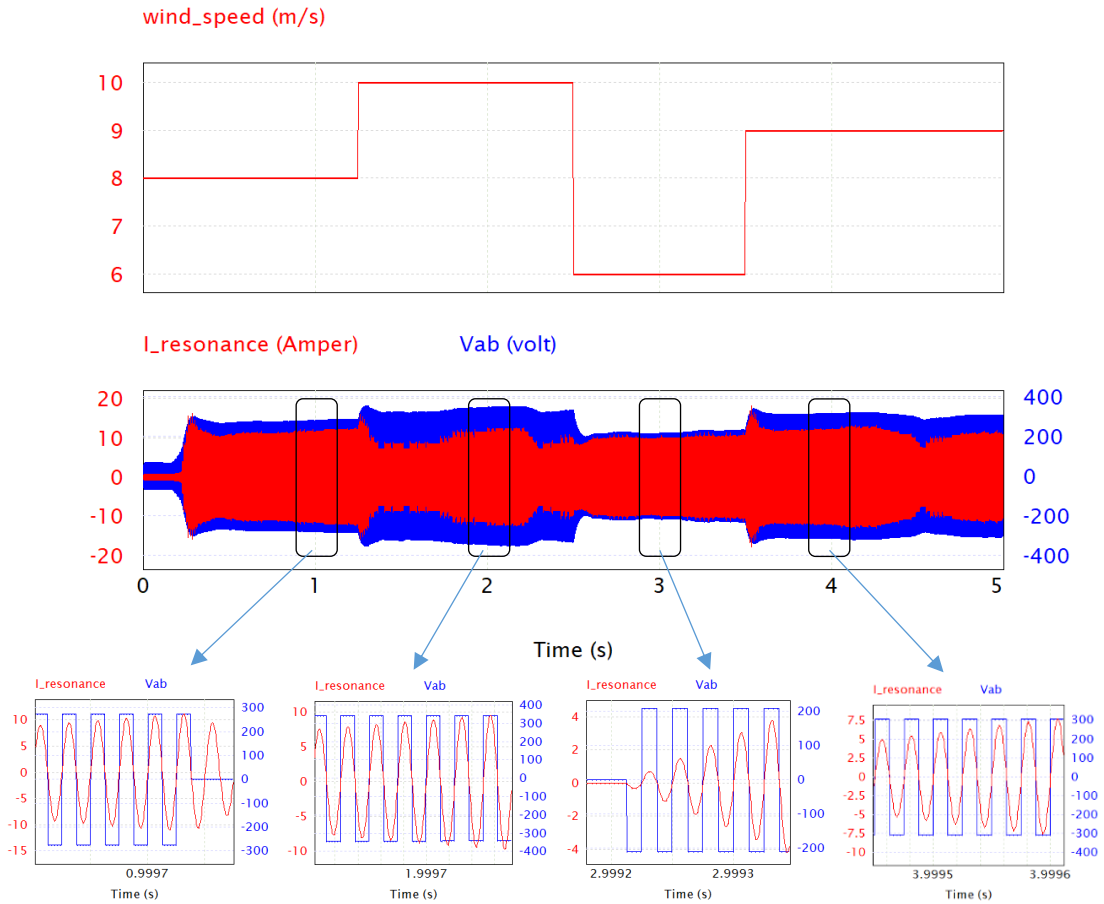

Figure 12. Inverter output voltage and resonant current.

5. CONCLUSIONS

This study analyzes the operation of a direct-drive WECS using a PMSG under soft switching conditions. The proposed method is centered on operating the SRDC at its resonant frequency by utilizing the PDM technique. By choosing the f_{sw} to match the f_r, switching of the power devices at zero current for all wind speeds is achieved, thereby minimizing switching losses. The MPPT process for 1.5 kW WECS has been performed using a sensorless control method, and the simulation results have been analyzed. The speed and power information required by the P&O algorithm used for MPPT was determined using the DSOGI-FLL method. The average error value of the estimated speed and power is below then 3%, indicating that the DSOGI-FLL algorithm's speed and power estimation is very close to reality. The simulation results present the current and voltage curves during the switching and isolation states of the upper and lower power switches. Power switches have maintained soft switching conditions across the entire wind speed profile. Furthermore, the sensorless control method employed in the designed system eliminates the need for auxiliary sensors, which reduces hardware costs and minimizes system complexity by streamlining the design process and eliminating potential sensor calibration issues. This cost-effective approach is particularly advantageous for small-power WECS applications, where budget constraints are critical. The proposed method also provides a theoretical foundation and simulation analysis, offering a detailed framework for operating a small-power WECS with enhanced efficiency, reliability, and power density.

ACKNOWLEDGEMENT

This research is supported by TUBITAK Research Fund (Project Number: 123E370) in Turkey.

This study is derived from the doctoral thesis titled “Değişken hızlı rüzgâr türbinleri için rezonans güç dönüştürücülü maksimum güç noktası izleyici geliştirilmesi” prepared at the Institue of Graduate Programs Karabük University

DECLARATION OF ETHICAL STANDARDS

The authors of this article declare that the materials and methods used in this study do not require ethical committee permission and/or legal-special permission.

AUTHOR’S CONTRIBUTIONS

Tufan Volkan KÜÇÜK: Wrote the manuscript and analyse the results.

Selim ÖNCÜ: Wrote the manuscript and analyse the results.

CONFLICT OF INTEREST

There is no conflict of interest in this study.

REFERENCES

[1] Song G., Cao B., and Chang L., “Advanced soft stall control for protection of small-scale wind generation systems”, ***IEEE Journal of Emerging and Selected Topics in Power Electronics***, 10(1): 273-284, (2021).

[2] Chen H., Xu D., and Deng, X., “Control for power converter of small-scale switched reluctance wind power generator”, ***IEEE Transactions on Industrial Electronics***, 68(4): 3148-3158, (2020).

[3] Mennad M., Bentaallah A., Djerırı Y., Ameur A. ve Bessas A.,“ Design of a standalone hybrid power system and optimization control with intelligent MPPT algorithms”, ***Politeknik Dergisi***, 27(1): 153-167, (2024).

[4] N. Nassir, B. Acar, and A. K. A. Fahed, “Vertical Axis Wind Turbine Installation Based on Wind Data Collected in Gharyan City, Libya”, ***Politeknik Dergisi,*** 25(3): 975–984, (2022).

[5] Zhang Z., Zhao Y., Qiao W. and Qu L., "A discrete-time direct torque control for direct-drive PMSG-based wind energy conversion systems", ***IEEE Transactions on Industry Applications***, 51(4): 3504-3514, (2015).

[6] Musarrat M. N., Islam M. R., Muttaqi K. M. and Sutanto D., "Enhanced frequency support from a PMSG-based wind energy conversion system integrated with a high temperature SMES in standalone power supply systems", ***IEEE Transactions on Applied Superconductivity***, 29(2): 1-6, (2018).

[7] Selamoğulları U.S., “Yenilenebilir enerji kaynaklarına sahip bir evin talep karakteristiğine uygun bir inverter tasarımının incelenmesi”, ***Politeknik Dergisi***, 23(2): 257-265, (2020).

[8] Urtasun A., Sanchis P. and Marroyo L., "Small wind turbine sensorless MPPT: robustness analysis and lossless approach", ***IEEE Transactions on Industry Applications***, 50(6): 4113-4121, (2014).

[9] De Oliveira Filho H. M., Oliveira D. D. S. and e Silva C. E. D. A., "Three-stage static power converter for battery charging feasible for small wind energy conversion systems", ***IEEE Transactions on Industry Applications***, 50(5): 3602-3610, (2014).

[10] Sejati P., Suzuki H. and Yasuno T., "Two-phase buck converter for battery charger of small scale wind turbine power system", ***International Electronics Symposium (IES)***, 244-247, (2016).

[11] Doshi K. and Joshi S., "Cascaded PI Controller based Wind Turbine Generator System for Battery Charging Applications", ***IEEE International Power and Renewable Energy Conference (IPRECON)***, 1-8, (2021).

[12] Kermani A. Y., Fadaeinedjad R., Maheri A., Mohammadi E. and Moschopoulos G., "Stall control and MPPT for a wind turbine, using a Buck converter in a battery storage system", ***IEEE Canadian Conference on Electrical and Computer Engineering (CCECE)***, 1-4, (2020).

[13] Abdelsalam I., Alajmi B. N., Marei M. I. and Alhajri M. F., "Wind energy conversion system based on open-end winding three-phase PMSG coupled with ac− dc buck-boost converter", ***The Journal of Engineering***, 2019(17): 4336-4340, (2019).

[14] Housseini B., Okou A. F. and Beguenane R., "Robust nonlinear controller design for on-grid/off-grid wind

energy battery-storage system", ***IEEE Transactions on Smart Grid***, 9(6): 5588-5598, (2017).

[15] Sharifi S., Monfared M., Babaei M. and Pourfaraj A., "Highly efficient single-phase buck–boost variable-frequency AC–AC converter with inherent commutation capability", ***IEEE Transactions on Industrial Electronics***, 67(5): 3640-3649, (2019).

[16] Hussain J. and Mishra M. K., "Adaptive maximum power point tracking control algorithm for wind energy conversion systems", ***IEEE Transactions on Energy Conversion***, 31(2): 697-705, (2016).

[17] Abbasi M. and Lam J., "An SiC-driven modular step-up converter with soft-switched module having 1: 1 turns ratio multiphase transformer for wind systems", ***IEEE Transactions on Industrial Electronics***, 66(9): 7055-7066, (2018).

[18] Abbasi M. and Lam J., "A new three-phase AC/DC high power factor soft-switched step-up converter with high gain rectifier modules for medium voltage grid in wind systems", ***IEEE Energy Conversion Congress and Exposition (ECCE)***, 1-8, (2016).

[19] Parastar A. and Seok J. K., "High-gain resonant switched-capacitor cell-based DC/DC converter for offshore wind energy systems", ***IEEE transactions on power electronics***, 30(2): 644-656, (2014).

[20] Dincan C., Kjaer P., Chen Y. H., Munk-Nielsen S. and Bak C. L., "A high-power, medium-voltage, series-resonant converter for DC wind turbines", ***IEEE Transactions on Power Electronics***, 33(9): 7455-7465, (2017).

[21] Fan S., Ma W., Lim T. C. and Williams B. W., "Design and control of a wind energy conversion system based on a resonant dc/dc converter", ***IET Renewable Power Generation***, 7(3): 265-274, (2013).

[22] Liao Y. H. and Dai Z. J., "Two-switch three-phase LLC resonant circuit with power factor correction for microscale wind power generation system", ***IEEE International Conference on Industrial Electronics for Sustainable Energy Systems (IESES)***, 382-388, (2018).

[23] Yeh C. S., Chen C. W., Lee M. and Lai J. S., "A hybrid modulation method for single-stage soft-switching inverter based on series resonant converter", ***IEEE Transactions on Power Electronics***, 35(6): 5785-5796, (2019).

[24] Wei Y., Luo Q. and Mantooth A., "Overview of modulation strategies for LLC resonant converter", ***IEEE Transactions on Power Electronics***, 35(10): 10423-10443, (2020).

[25] Deshmukh S., Iqbal A., Islam S., Khan I., Marzband M., Rahman S. and Al-Wahedi A. M., "Review on classification of resonant converters for electric vehicle application", ***Energy reports***, 8: 1091-1113, (2022).

[26] Unal K., Bal G., Oncu S. and Ozturk N., "MPPT Design for PV-Powered WPT System with Irregular Pulse Density Modulation", ***Electric Power Components and Systems***, 51(1): 83-91, (2023).

[27] Singh K. A., Chaudhary A. and Chaudhary K., "Three-phase AC-DC Converter for Direct-drive PMSG-based Wind Energy Conversion System", ***Journal of Modern Power Systems and Clean Energy***, 11(2): 589-598, (2022).

[28] Kucuk T. V. and Oncu S., "Wind Energy Conversion System With PDM Controlled Converter", ***10th International Conference on Renewable Energy Research and Application (ICRERA)***, 136-140, (2021).

[29] Zhang Z., Zhao Y., Qiao W. and Qu L., "A space-vector-modulated sensorless direct-torque control for direct-drive PMSG wind turbines", ***IEEE Transactions on Industry Applications***, 50(4): 2331-2341, (2014).

[30] Unal K., Oncu S., Tuncer U. and Bal G., "Determination of Circuit Parameters in Domestic Induction Heaters by Analytical Solution Method", ***Electric Power Components and Systems***, 1-9, (2024).

[31] Özbay H., "PDM-MPPT based solar powered induction heating system", ***Engineering Science and Technology, an International Journal***, 23(6): 1397-1414, (2020).

[32] Özbay H., Karafil A. and Öncü S., "Sliding mode PLL-PDM controller for induction heating system", ***Turkish Journal of Electrical Engineering and Computer Sciences***, 29(2): 1241-1258, (2021).

[33] Nguyen A. T. and Lee D. C., "Sensorless control of DFIG wind turbine systems based on SOGI and rotor position correction", ***IEEE Transactions on Power Electronics***, 36(5): 5486-5495, (2020).

[34] Karthik M. and Panda A. K., "Enhancement of Power Quality in a Grid-Connected Photovoltaic System using Robust Modified Champernowne Function Adaptive Filter and DSOGI-FLL", ***IEEE 3rd International Conference on Smart Technologies for Power, Energy and Control (STPEC)***, 1-6, (2023).

[35] Dao N. D., Lee D. C. and Lee S., "A simple and robust sensorless control based on stator current vector for PMSG wind power systems", ***IEEE Access***, 7: 8070-8080, (2018).

[36] Patil K. and Patel H. H., "Modified SOGI based shunt active power filter to tackle various grid voltage abnormalities", ***Engineering Science and Technology, an International Journal***, 20(5): 1466-1474, (2017).

[37] Nazib A. A., Holmes D. G. and McGrath B. P., "Decoupled DSOGI-PLL for improved three phase grid synchronisation", ***International Power Electronics Conference (IPEC-Niigata 2018-ECCE Asia)***, 3670-3677, (2018).

[38] Kherbachi A., Bendib A., Kara K. and Chouder A., "ARM based implementation of SOGI-FLL method for power calculation in single-phase power system", ***5th International Conference on Electrical Engineering-Boumerdes (ICEE-B)***, 1-6, (2017).

[39] Shutari H., Ibrahim T., Nor N. B. M., Saad N., Tajuddin M. F. N. and Abdulrab H. Q., "Development of a novel efficient maximum power extraction technique for grid-tied VSWT system", ***IEEE Access***, 10: 101922-101935, (2022).

[40] Yazıcı İ., and Yaylacı, E. K, "Modified grey wolf optimizer based MPPT design and experimentally performance evaluations for wind energy systems", ***Engineering Science and Technology, an International Journal***, *46*: 101520, (2023).

[41] M. Mabrouk, B. Abderrahim, Y. Djeriri, A. Ameur, and A. Bessas, "Design of a Standalone Hybrid Power System and Optimization Control with Intelligent MPPT Algorithms", ***Politeknik Dergisi***, 27(1), 153–167, (2024).